Global Asymptotic Stability of Current-Controlled Modular Multilevel Converters

Lennart Harnefors, *Senior Member, IEEE*, Antonios Antonopoulos, *Student Member, IEEE*, Kalle Ilves, *Student Member, IEEE*, and Hans-Peter Nee, *Senior Member, IEEE*

***Abstract*—In this paper, previously developed stability results for open-loop sum-capacitor-voltage control of modular multilevel converters are extended. To give improved damping, circulating-current feedback is included in the control law. With the output-current control loop and a first-order measurement lag taken into account, global asymptotic stability is proven. Careful consideration of the on-line sum-capacitor-voltage reference computation is given, since this is the most critical part of the control system.**

***Index Terms*—Converters, current control, Lyapunov methods, multilevel systems.**

NOMENCLATURE

The upper and lower arms of the converter, cf. Fig. 1(b), are denoted with the subscripts "u" and "l," respectively. An expression which is valid for either of the arms is denoted with the subscript "u,l." The subscript "m" denotes measured value (via a lag).

M	Number of phases.
N	Number of submodules per arm.
C	Submodule capacitance.
L	Arm inductance.
R	Parasitic arm resistance.
v_d	DC-bus voltage.
i_d	DC-bus current.
$v^i_{cu,l}$,	$i = 1, \ldots, N$ Individual capacitor voltages.
$v^\Sigma_{cu,l}$	$= \sum_{i=1}^{N} v^i_{cu,l}$ Sum capacitor voltages.
$n_{u,l}$	Insertion indices.
$v_{cu,l}$	$= n_{u,l} v^\Sigma_{cu,l}$ Inserted voltages.
$i_{u,l}$	Arm currents.
i_s	$= i_u - i_l$ Output current.
i_c	$= (i_u + i_l)/2$ Circulating current.
v_s	$= (v_{cl} - v_{cu})/2$ Output voltage (driving i_s).
v_c	$= (v_d - v_{cu} - v_{cl})/2$ Internal voltage (driving i_c).
v_g	Grid voltage.
ω_1	Fundamental angular frequency.
*	Reference value.
$\sim$	Error value.

Manuscript received September 28, 2013; revised November 14, 2013; accepted January 4, 2014. Date of publication January 9, 2014; date of current version August 26, 2014. This work was supported in part by Elforsk, in part by Energimyndigheten, and in part by ABB. Recommended for publication by Associate Editor Prof. M. Tavakoli Bina.

L. Harnefors is with the ABB Corporate Research, Västerås, Sweden, and with the Royal Institute of Technology (KTH), SE-100 44 Stockholm, Sweden (e-mail: lennart.harnefors@se.abb.com).

A. Antonopoulos, K. Ilves, and H.-P. Nee are with the Royal Institute of Technology (KTH), SE-100 44 Stockholm, Sweden (e-mail: anta@kth.se; ilves@kth.se; hansi@kth.se).

Digital Object Identifier 10.1109/TPEL.2014.2298560

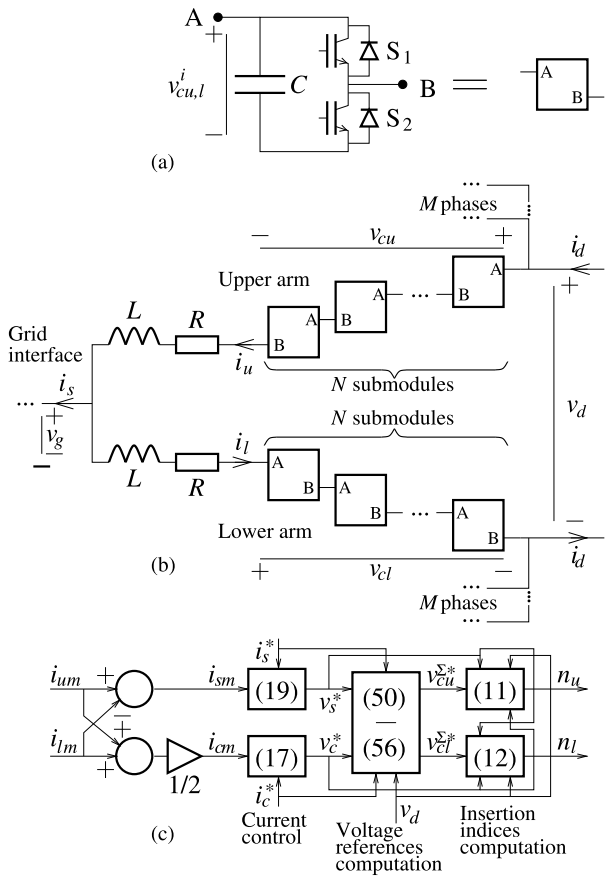

Fig. 1. (a) Submodule and (b) circuit diagram of a modular multilevel converter (MMC); (c) control-system block diagram with references to equations.

I. INTRODUCTION

MMCs (also known as M2Cs or M2LCs) [3]–[10] have many attractive properties, notably low-harmonic content of the output voltage, high efficiency, and scalability in terms of voltage levels [11], [12]. The MMC consists of N identical series-connected submodules (also called cells) per arm, cf. Fig. 1. The controllable semiconductor device in each switch S_1 and S_2 in Fig. 1(a) may be an insulated-gate bipolar transistor. The MMC is well suited for high-voltage high-power applications, such as high-voltage dc transmission [11]–[13] (where N may be as high as several hundred), high-power motor drives [14]–[17], and electric railway supplies [18], [19]. The basic operation was described thoroughly in [3]–[10], and [20]. Descriptions of the internal dynamics were presented in [21]–[23], and control schemes were proposed in [21], [23]–[26], and [27].

The so-called open-loop control principle of the MMC was introduced in [24]. The benefits of this scheme are that the capacitor-voltage measurement is not needed for the higher level control (only for capacitor-voltage balancing), that an asymptotically stable system is obtained without the addition of explicit sum-capacitor-voltage control loops, and that a second-order harmonic in the circulating current is avoided (or at least is significantly reduced). Local asymptotic stability was shown by means of small-signal analysis under some simplifying assumptions in [27]. Global asymptotic stability was shown through Lyapunov theory in [28], thus strengthening the stability properties.

Circulating-current control may greatly improve the damping of the system [27]. Unfortunately, the proof of global stability in [28] did not consider circulating-current control. In addition, only the internal dynamics, i.e., the system comprising the sum capacitor voltages and the circulating current, was taken into account; the output current was considered static. Neither was the impact of a lag caused by time delays and/or antialiasing low-pass filters in the measurement systems for the arm currents (from which the circulating and output currents are calculated) considered in [27].

The contribution of this paper is the exploration of the mentioned disregarded issues. In Section II, the output current is included in an extended per-phase dynamic model and closed-loop control of the circulating and output currents is considered. A first-order lag is included in both current control loops to model measurement-system imperfections.

For the given assumptions, it is shown in Section III, using Lyapunov theory, that the resulting dynamic system is globally asymptotically stable. This is a direct extension of the proof presented in [28].

The on-line computation of the sum-capacitor-voltage references must be implemented with care for the stability proof to hold in practice. This is the most critical part of the scheme, to which Section IV is devoted.

Finally, Section V presents some simulations and experimental results which vindicate the results in a practical environment.

Preliminary results were presented in [29].

II. Dynamic Model and Control Method

A. Per Phase Dynamics

We shall here briefly summarize the derivation of a continuous-time model. A thorough derivation, which shows all intermediate steps, can be found in [27]. Fig. 1(c) shows a block diagram of the proposed control system.

It is assumed that the individual capacitor-voltage sharing within each arm is maintained by a selection mechanism as described in [6] and [24]. The switching frequency and the number of submodules per arm are assumed to be sufficiently high to make discrete effects negligible as compared with the waveform amplitude. These assumptions allow the insertion indices to be considered continuous on the interval $[0, 1]$. As a result thereof, the inserted voltages too can be considered as continuous variables.

As argued in [27], a stiff dc-bus voltage v_d can be assumed. In addition, we shall in this paper assume also a stiff grid (ac-bus) voltage v_g. These assumptions allow each phase leg of the converter to be treated separately, and makes the theory general for any number of phases M. All equations are therefore given per phase, and explicit phase notation is not used.

By considering the total arm energy, as shown in [27], the definitions made in the Nomenclature, and the circuit diagram depicted in Fig. 1(b), the following fourth-order representation of the per-phase dynamics is obtained:

$$\frac{dv_{cu}^{\Sigma}}{dt} = \frac{Nn_u}{C} i_u \tag{1}$$

$$\frac{dv_{cl}^{\Sigma}}{dt} = \frac{Nn_l}{C} i_l \tag{2}$$

$$\frac{di_c}{dt} = \frac{1}{L}\left(v_c - Ri_c\right) \tag{3}$$

$$\frac{di_s}{dt} = \frac{2}{L}\left(v_s - v_g - \frac{R}{2} i_s\right) \tag{4}$$

of which (1)–(3) comprise the so-called internal dynamics [27], [28]. Using the definitions of i_s, i_c, v_c, and v_s in the Nomenclature allows us to rewrite these relations as

$$\frac{dv_{cu}^{\Sigma}}{dt} = \frac{Nn_u}{C}\left(\frac{i_s}{2} + i_c\right) \tag{5}$$

$$\frac{dv_{cl}^{\Sigma}}{dt} = \frac{Nn_l}{C}\left(-\frac{i_s}{2} + i_c\right) \tag{6}$$

$$\frac{di_c}{dt} = \frac{1}{L}\left(\frac{v_d - n_u v_{cu}^{\Sigma} - n_l v_{cl}^{\Sigma}}{2} - Ri_c\right) \tag{7}$$

$$\frac{di_s}{dt} = \frac{2}{L}\left(\frac{-n_u v_{cu}^{\Sigma} + n_l v_{cl}^{\Sigma}}{2} - v_g - \frac{R}{2} i_s\right). \tag{8}$$

B. Open-Loop Voltage Control

From the definitions made in the Nomenclature, the following voltage relations are found:

$$v_{cu} = n_u v_{cu}^{\Sigma} = \frac{v_d}{2} - v_s - v_c \tag{9}$$

$$v_{cl} = n_l v_{cl}^{\Sigma} = \frac{v_d}{2} + v_s - v_c. \tag{10}$$

By solving (9) and (10) for n_u and n_l, respectively, and substituting v_s and v_c with their references $v_s^{\star}$ and $v_c^{\star}$, selections of the insertion indices which compensate for the sum-capacitor-voltage ripples are found, such that $v_s = v_s^{\star}$ and $v_c = v_c^{\star}$ (ideally, at least). However, the resulting closed-loop system will be marginally stable [27]. Voltage control loops need to be added to achieve asymptotic stability [21], [23]. By adopting instead the open-loop approach of [24], i.e., substituting also v_{cu}^{Σ} and v_{cl}^{Σ} with their respective references $v_{cu}^{\Sigma\star}$ and $v_{cl}^{\Sigma\star}$, an asymptotically stable system is obtained without the addition of voltage control loops [27], [28]. The so obtained insertion indices are given as

$$n_u = \frac{v_d/2 - v_s^{\star} - v_c^{\star}}{v_{cu}^{\Sigma\star}} \tag{11}$$

$$n_l = \frac{v_d/2 + v_s^{\star} - v_c^{\star}}{v_{cl}^{\Sigma\star}}. \tag{12}$$

The sum-capacitor-voltage references are obtained from (5) and (6) by substituting $v_{cu,l}^{\Sigma} \to v_{cu,l}^{\Sigma\star}$, $i_c \to i_c^\star$, and $i_s \to i_s^\star$, where $i_c^\star$ and $i_s^\star$ are the respective references for i_c and i_s. That is

$$\frac{dv_{cu}^{\Sigma\star}}{dt} = \frac{Nn_u}{C}\left(\frac{i_s^\star}{2} + i_c^\star\right) \tag{13}$$

$$\frac{dv_{cl}^{\Sigma\star}}{dt} = \frac{Nn_l}{C}\left(-\frac{i_s^\star}{2} + i_c^\star\right). \tag{14}$$

The on-line computation of (13) and (14) is the core of the control scheme and requires care in its implementation. See Section IV for details.

C. Current Control Loops

One of the benefits of the open-loop voltage control approach is that the internal dynamics become insensitive to measurement lags [24]. One drawback, on the other hand, is that the damping of the internal dynamics are solely determined by the parasitic arm resistance R. As the latter should be as small as possible to give as high an efficiency as possible, the damping will generally be poor [27]. To improve the damping, a proportional feedback of the circulating current can be included in the selection of $v_c^\star$ [27]. The control scheme is then no longer purely open loop, which the on-line computation of (13) and (14) must take into account. See Section IV.

In the stability analysis performed in [28], the output-current dynamics were disregarded, but are included in the analysis to follow. Neither was a measurement lag considered in [28]. This is now rectified by the inclusion of a first-order lag with bandwidth α_m, i.e., with transfer function

$$H_m(s) = \frac{\alpha_m}{s + \alpha_m}. \tag{15}$$

The measured circulating and output currents are thus given by

$$i_{cm} = H_m(s) i_c \qquad i_{sm} = H_m(s) i_s \tag{16}$$

where here, and in other similar relations, $s = d/dt$. Since the circulating current ideally shall be constant and $H_m(0) = 1$, i_{cm} can immediately be used in a circulating-current control law

$$v_c^\star = R_a(i_c^\star - i_{cm}) + Ri_c^\star, \qquad i_c^\star = \frac{i_d}{M} \tag{17}$$

where the feedforward (second) term is a compensation for the resistive voltage drop in (3). The notation R_a of the proportional gain in the feedback (first) term is so chosen, since it can be regarded as an "active resistance." Its impact on the system dynamics was investigated in [27].

The output current, on the other hand, shall be a fundamental-frequency sinusoid. As a result, the measurement lag will incur static amplitude and phase errors. Since the current control law will be designed such that $i_s = i_s^\star$ in the steady state, an adequate compensation for these errors is given by

$$i'_{sm} = \underbrace{H_m(s) i_s}_{i_{sm}} + \underbrace{[1 - H_m(s)] i_s^\star}_{i_{\mathrm{comp}}}. \tag{18}$$

The compensation term i_{comp} is constructed as high-pass filtering of the output-current reference. Note that if $i_s = i_s^\star$, then $i'_{sm} = i_s = i_s^\star$. The compensated current i'_{sm} can be used in an output-current control law as

$$v_s^\star = \frac{\alpha_c L}{2}(i_s^\star - i'_{sm}) + H_1(s)\left[\frac{R + sL}{2} i_s^\star + v_g\right]. \tag{19}$$

This control law consists of a proportional feedback term with gain $\alpha_c L/2$ (which ideally gives a closed-loop system with bandwidth α_c [30]) and a feedforward term, which employs a bandpass filter $H_1(s)$ centered at the fundamental frequency and with bandwidth α_f. This is a special case ($h = 1$) of the general harmonic bandpass filter

$$H_h(s) = \frac{\alpha_f s}{s^2 + \alpha_f s + (h\omega_1)^2}. \tag{20}$$

In the feedforward of $i_s^\star$—unlike that of $i_c^\star$ in (17)—the full impedance $(R + sL)/2$ has to be included; as $i_s^\star$ is a sinusoid, a static error would result if term sL were omitted. Together with a feedforward of the grid voltage [31], a static error is then avoided without the addition of a resonant part [32] to the control law.

Remark 1: For a three-phase converter, current control is normally not made per phase, but using space vectors in a stationary ($\alpha\beta$) or synchronous (dq) reference frame [30]. In that case, (18) can be replaced by a complex gain, giving the correct steady-state amplitude and phase compensation. As long as additional (integral and/or resonant) parts are not added to the control law, the stability analysis to be made in the next section holds also for space-vector output-current control.

III. Stability Analysis

After setting the stage, we shall in this section rigorously establish global asymptotic stability using Lyapunov theory.

A. Assumptions

As mentioned previously, stiff dc-bus and grid voltages are assumed. In addition, the dynamics of any outer loops, e.g., for active- and reactive-power control, are assumed to be much slower than the per-phase dynamics. This makes it reasonable for:

1) v_d and $i_c^\star$ to be assumed constant;
2) v_g and $i_s^\star$ to be assumed as static fundamental-frequency sinusoids.

This, in turn, allows the bandpass filter in (19) to be disregarded; since $H_1(j\omega_1) = 1$, it does not have an impact on static fundamental-frequency signals. The following output-current control law thus can be considered:

$$v_s^\star = \frac{\alpha_c L}{2}(i_s^\star - i'_{sm}) + \frac{R}{2} i_s^\star + \frac{L}{2}\frac{di_s^\star}{dt} + v_g. \tag{21}$$

B. Error Dynamics

As will now be shown, the system dynamics derived in Section II can be reduced to a nonlinear and time-varying sixth-order dynamic system in the error (deviation) variables

$$\begin{aligned} \tilde{v}_{cu}^{\Sigma} &= v_{cu}^{\Sigma} - v_{cu}^{\Sigma\star} \quad \tilde{v}_{cl}^{\Sigma} = v_{cl}^{\Sigma} - v_{cl}^{\Sigma\star} \\ \tilde{i}_c &= i_c - i_c^\star \quad \tilde{i}_{cm} = i_{cm} - i_c^\star \\ \tilde{i}_s &= i_s - i_c^\star \quad \tilde{i}_{sm} = i'_{sm} - i_c^\star. \end{aligned} \tag{22}$$

Subtracting (13) from (5) and (14) from (6), the equations governing the sum-capacitor-voltage errors are obtained as

$$\frac{d\tilde{v}_{cu}^{\Sigma}}{dt} = \frac{Nn_u}{C}\left(\frac{\tilde{i}_s}{2} + \tilde{i}_c\right) \tag{23}$$

$$\frac{d\tilde{v}_{cl}^{\Sigma}}{dt} = \frac{Nn_l}{C}\left(-\frac{\tilde{i}_s}{2} + \tilde{i}_c\right). \tag{24}$$

Somewhat more complicated manipulations are needed to obtain a corresponding relation for the circulating-current error. Substituting (22) into (7) yields, as $di_c^{\star}/dt = 0$

$$\frac{d\tilde{i}_c}{dt} = \frac{1}{L}\left[\frac{v_d - n_u(v_{cu}^{\Sigma\star} + \tilde{v}_{cu}^{\Sigma}) - n_l(v_{cl}^{\Sigma\star} + \tilde{v}_{cl}^{\Sigma})}{2} - R(\tilde{i}_c + i_c^{\star})\right]. \tag{25}$$

Using (11) and (12) allows (25) to be simplified as

$$\frac{d\tilde{i}_c}{dt} = \frac{1}{L}\left[-\frac{n_u\tilde{v}_{cu}^{\Sigma} + n_l\tilde{v}_{cl}^{\Sigma}}{2} + v_c^{\star} - R(\tilde{i}_c + i_c^{\star})\right] \tag{26}$$

and substitution of (17) into (26) results in

$$\frac{d\tilde{i}_c}{dt} = -\frac{1}{L}\left(\frac{n_u\tilde{v}_{cu}^{\Sigma} + n_l\tilde{v}_{cl}^{\Sigma}}{2} + R_a\tilde{i}_{cm} + R\tilde{i}_c\right). \tag{27}$$

It is easily verified that the first relation in (16) equivalently can be expressed as

$$\frac{d\tilde{i}_{cm}}{dt} = \alpha_m(\tilde{i}_c - \tilde{i}_{cm}). \tag{28}$$

The equation governing the output-current error is obtained by making similar manipulations of (8) as were made of (7), resulting in

$$\frac{d(\tilde{i}_s + i_s^{\star})}{dt} = \frac{2}{L}\left[\frac{-n_u\tilde{v}_{cu}^{\Sigma} + n_l\tilde{v}_{cl}^{\Sigma}}{2} + v_s^{\star} - v_g - \frac{R}{2}(\tilde{i}_s + i_s^{\star})\right]. \tag{29}$$

Substitution of (21) into (29) then yields

$$\frac{d\tilde{i}_s}{dt} = \frac{2}{L}\left(\frac{-n_u\tilde{v}_{cu}^{\Sigma} + n_l\tilde{v}_{cl}^{\Sigma}}{2} - \frac{\alpha_c L}{2}\tilde{i}_{sm} - \frac{R}{2}\tilde{i}_s\right). \tag{30}$$

Finally, multiplying (18) by $(s + \alpha_m)$, we get

$$\begin{aligned}(s+\alpha_m)i'_{sm} &= \alpha_m i_s + s i_s^{\star} \Rightarrow \\ \frac{d(i'_{sm} - i_s^{\star})}{dt} &= \alpha_m(i_s - i'_{sm}) \Rightarrow \\ \frac{d\tilde{i}_{sm}}{dt} &= \alpha_m(\tilde{i}_s - \tilde{i}_{sm}).\end{aligned} \tag{31}$$

The error system consisting of (23), (24), (27), (28), (30), and (31) can be expressed in a compact state-space form by introducing $\tilde{x} = [\tilde{v}_{cu}^{\Sigma}, \tilde{v}_{cl}^{\Sigma}, \tilde{i}_c, \tilde{i}_{cm}, \tilde{i}_s, \tilde{i}_{sm}]^T$, giving

$$\dot{\tilde{x}} = A\tilde{x} \tag{32}$$

where

$$A = \begin{bmatrix} 0 & 0 & \frac{Nn_u}{C} & 0 & \frac{Nn_u}{2C} & 0 \\ 0 & 0 & \frac{Nn_u}{C} & 0 & -\frac{Nn_u}{2C} & 0 \\ -\frac{n_u}{2L} & -\frac{n_l}{2L} & -\frac{R}{L} & -\frac{R_a}{L} & 0 & 0 \\ 0 & 0 & \alpha_m & -\alpha_m & 0 & 0 \\ -\frac{n_u}{L} & \frac{n_l}{L} & 0 & 0 & -\frac{R}{L} & -\alpha_c \\ 0 & 0 & 0 & 0 & \alpha_m & -\alpha_m \end{bmatrix}. \tag{33}$$

C. Stability Proof

Although the structure of (32) is that of a linear, time-invariant system, state matrix A is time varying, since n_u and n_l, via (19), are functions of the sinusoids $i_s^{\star}$ and v_g, cf. (11) and (12). In addition, (32) is nonlinear, since n_u and n_l, via (17) and (19), are functions also of $\tilde{i}_{cm}$ and $\tilde{i}_{sm}$, i.e., of $\tilde{x}$.[1] Stability therefore cannot be investigated via the eigenvalues of A. Lyapunov theory, on the other hand, is powerful enough to tackle both time variations and nonlinearities [33]. The structure of (32) allows the search for a Lyapunov function candidate (LFC) of the form

$$V = \tilde{x}^T P\tilde{x}. \tag{34}$$

With a constant matrix P, we obtain, using (32)

$$\begin{aligned}\dot{V} &= \dot{\tilde{x}}^T P\tilde{x} + \tilde{x}^T P\dot{\tilde{x}} = -\tilde{x}^T Q\tilde{x}, \\ Q &= -(A^T P + PA).\end{aligned} \tag{35}$$

The stage is now set to allow the formulation of the following theorem.

Theorem: System (32) is globally asymptotically stable about $\tilde{x} = 0$ if

1) C, L, N, R_a, α_c, and α_m are positive constants, and
2) R is positive and may be time varying.

Proof: Consider an LFC of the form (34), with

$$P = \mathrm{diag}\left(\frac{C}{4N}, \frac{C}{4N}, \frac{L}{2}, \frac{R_a}{2\alpha_m}, \frac{L}{8}, \frac{L\alpha_c}{8\alpha_m}\right). \tag{36}$$

P is positive definite, so (34) is radially unbounded and positive, except at $\tilde{x} = 0$ where $V = 0$. Since P is constant, $\dot{V}$ can be calculated according to (35). It is immediately verified that

$$Q = \mathrm{diag}\left(0, 0, R, R_a, \frac{R}{4}, \frac{\alpha_c L}{4}\right) \tag{37}$$

which is positive semidefinite. Thus, (34) is a global Lyapunov function, implying that (32) is globally stable. Asymptotic stability follows from LaSalle's invariance principle [33] in a similar fashion as in [28]. In component form, (35) can be expressed as

$$\dot{V} = -\left(R\tilde{i}_c^2 + R_a\tilde{i}_{cm}^2 + \frac{R}{4}\tilde{i}_s^2 + \frac{\alpha_c L}{4}\tilde{i}_{sm}^2\right). \tag{38}$$

[1] Perfectly strict notation of (32) would be $\dot{\tilde{x}}(t) = A[t, \tilde{x}(t)]\tilde{x}(t)$, which is avoided in order not to introduce further notational clutter.

Since all coefficients within the parentheses in (38) are positive, $\dot{V} \equiv 0$ implies $\tilde{i}_c \equiv \tilde{i}_{cm} \equiv \tilde{i}_s \equiv \tilde{i}_{sm} \equiv 0$. Substitution thereof in (23), (24), (27), and (30) results in

$$\frac{d\tilde{v}_{cu}^{\Sigma}}{dt} \equiv 0 \tag{39}$$

$$\frac{d\tilde{v}_{cl}^{\Sigma}}{dt} \equiv 0 \tag{40}$$

$$0 \equiv n_u \tilde{v}_{cu}^{\Sigma} + n_l \tilde{v}_{cl}^{\Sigma} \tag{41}$$

$$0 \equiv -n_u \tilde{v}_{cu}^{\Sigma} + n_l \tilde{v}_{cl}^{\Sigma}. \tag{42}$$

From (39) and (40) it follows that $\tilde{v}_{cu}^{\Sigma}$ and $\tilde{v}_{cl}^{\Sigma}$ both must be constant. However, since n_u and n_l are time varying and not linearly related, the only constants $\tilde{v}_{cu}^{\Sigma}$ and $\tilde{v}_{cl}^{\Sigma}$ that satisfy (41) and (42) are $\tilde{v}_{cu}^{\Sigma} \equiv \tilde{v}_{cl}^{\Sigma} \equiv 0$. Consequently, (32) is globally asymptotically stable.

Remark 2: Obviously, the assumptions on which the proof is based represent a somewhat idealized situation. These implicitly include that R and L are perfectly known, via the feedforward terms in control laws (17) and (19). Although some deviations from the true values cannot be avoided, L normally does not exhibit significant variations (unless iron-core arm inductors are used, which may saturate), whereas R normally is small. Therefore, there is normally no impact on system stability and only slight impact on voltage and current control accuracy (see Section V). Another idealized assumption is implied by the reference-voltage computations (13) and (14), which need to be modified as shown in the next section.

IV. Arm-Energy and Sum-Capacitor-Voltage Reference Computation

We shall now direct our attention to the reference-computation relations (13) and (14), which are rearranged as follows. First, (11) and (12) are, respectively, substituted into (13) and (14), which respectively are multiplied by $v_{cu}^{\Sigma\star}$ and $v_{cl}^{\Sigma\star}$. The arm-energy references

$$W_{u,l}^{\star} = \frac{C}{2N}(v_{u,l}^{\Sigma\star})^2 \tag{43}$$

are then introduced, allowing (13) and (14) respectively to be simplified as

$$\frac{dW_u^{\star}}{dt} = \left(\frac{v_d}{2} - v_s^{\star} - v_c^{\star}\right)\left(\frac{i_s^{\star}}{2} + i_c^{\star}\right) \tag{44}$$

$$\frac{dW_l^{\star}}{dt} = \left(\frac{v_d}{2} + v_s^{\star} - v_c^{\star}\right)\left(-\frac{i_s^{\star}}{2} + i_c^{\star}\right). \tag{45}$$

In theory, the arm-energy references could be computed online as written, i.e., by direct integration of the right-hand sides of (44) and (45). In practice, though, this will invariably fail, since an open-loop integration gradually will build up a bias, resulting in flawed operation. In [24] and [28], this problem was circumvented for $R_a = 0$ and with the output-current dynamics disregarded by considering $v_s^{\star}$, $v_c^{\star} = Ri_c^{\star}$, and i_s as quasi-stationary quantities. Bias-free closed-form expressions for the arm-energy references could then be obtained. This option is no longer available, since the feedback terms of i_{cm} and i'_{sm} in, respectively, control laws (17) and (19) prevent closed-form expressions from being obtained.

Using a low-pass filter instead of a pure integrator may seem as a feasible solution. However, the bandwidth of the filter must be made very low to prevent unacceptably large phase errors from appearing. The dc-component suppression will then not be fast enough, resulting in deteriorating stability properties due to the tendency of bias buildup.

Bandpass filtering is the best approach found so far. A bandpass filter with transfer function (20) lets an hth-order harmonic component pass without amplitude or phase distortion, as $H_h(jh\omega_1) = 1$. To find out which bandpass filters to apply, the right-hand sides of (44) and (45) are analyzed further. To simplify the calculations, the total and imbalance arm-energy references

$$W_{\Sigma}^{\star} = W_u^{\star} + W_l^{\star}, \qquad W_{\Delta}^{\star} = W_u^{\star} - W_l^{\star} \tag{46}$$

are introduced in (44) and (45), which yields

$$\frac{dW_{\Sigma}^{\star}}{dt} = (v_d - 2v_c^{\star})i_c^{\star} - v_s^{\star} i_s^{\star} \tag{47}$$

$$\frac{dW_{\Delta}^{\star}}{dt} = (v_d - 2v_c^{\star})i_s^{\star}/2 - 2v_s^{\star} i_c^{\star}. \tag{48}$$

The product $v_s^{\star} i_s^{\star}$, i.e., of two fundamental-frequency variables, shows that the right-hand side of (47) has a frequency component at $2\omega_1$. For a three-phase converter, a third harmonic, whose amplitude should be set to one-sixth of the fundamental component, can be added to $v_s^{\star}$ to extend the modulation range [34]. This will add a frequency component at $4\omega_1$. It is immediately seen that the right-hand side of (48) has frequency components at ω_1 and (with a third harmonic added to $v_s^{\star}$) $3\omega_1$.

As integration corresponds to division by s, a frequency component at $h\omega_1$ in $W_{\Sigma}^{\star}$ or in $W_{\Delta}^{\star}$ can be extracted by filtering the signal corresponding to the right-hand side of (47) or (48) through

$$\frac{H_h(s)}{s} = \frac{\alpha_f}{s^2 + \alpha_f s + (h\omega_1)^2}. \tag{49}$$

Consequently, the sum-capacitor-voltage references can be obtained via the following steps:

1) The total and difference arm-energy ripples are estimated by filtering the right-hand sides of (47) and (48) as

$$\Delta W_{\Sigma}^{\star} = H_{\Sigma}(s)\left[(v_d - 2v_c^{\star})i_c^{\star} - v_s^{\star} i_s^{\star}\right] \tag{50}$$

$$\Delta W_{\Delta}^{\star} = H_{\Delta}(s)\left[(v_d - 2v_c^{\star})i_s^{\star}/2 - 2v_s^{\star} i_c^{\star}\right] \tag{51}$$

where

$$\begin{aligned} H_{\Sigma}(s) &= \frac{1}{s}[H_2(s) + H_4(s)] \\ &= \frac{\alpha_f}{s^2 + \alpha_f s + (2\omega_1)^2} + \frac{\alpha_f}{s^2 + \alpha_f s + (4\omega_1)^2} \\ H_{\Delta}(s) &= \frac{1}{s}[H_1(s) + H_3(s)] \\ &= \frac{\alpha_f}{s^2 + \alpha_f s + \omega_1^2} + \frac{\alpha_f}{s^2 + \alpha_f s + (3\omega_1)^2}. \end{aligned} \tag{52}$$

This filtering rejects all frequency components—including any dc bias—except those of interest, which pass virtually undistorted as long as $\alpha_f \ll \omega_1$. The latter restriction ensures a negligible interaction between the two band-pass filters in each pair. For example, $\alpha_f = 0.2\omega_1$ yields $H_1(j\omega_1) + H_3(j\omega_1) = 1.001e^{j1.4^\circ}$. On the other hand, this selection of α_f gives fast enough dc-component rejection, preventing the tendency to bias buildup.

2) To the ripple estimates, the mean references are added. Since (47) and (48) are open-loop integrations, these mean references can be regarded as integration constants, which can be selected freely. Normally, $W_\Delta^\star$ should have zero mean, i.e., balanced arm energies, so

$$W_\Sigma^\star = W_{\Sigma 0}^\star + \Delta W_\Sigma^\star, \qquad W_\Delta^\star = \Delta W_\Delta^\star. \tag{53}$$

Generally, the sum capacitor voltage in each arm should equal v_d, i.e., the mean per-arm energy should be $Cv_d^2/(2N)$. So, generally, the mean total energy reference should be selected as

$$W_{\Sigma 0}^\star = \frac{Cv_d^2}{N} \tag{54}$$

but any desired value can be chosen.

3) The arm-energy references are computed as

$$W_u^\star = \frac{W_\Sigma^\star + W_\Delta^\star}{2}, \qquad W_l^\star = \frac{W_\Sigma^\star - W_\Delta^\star}{2}. \tag{55}$$

4) Finally, the sum-capacitor-voltage references are obtained from the arm-energy references as

$$v_{cu,l}^\star = \sqrt{\frac{2N}{C} W_{u,l}^\star}. \tag{56}$$

Remark 3: Since the measured output and circulating currents are not used explicitly in the computations of the arm-energy references (only implicitly via the insertion indices), the proposed method is invariant of the measurement lag. On the other hand, it is sensitive to model parameter C; an inaccurate value will result in inaccurate ripple estimation. This sensitivity can, however, be reduced to a minimum. First, accurate capacitance measurement can be made when the converter is commissioned. Second, capacitances change due to ageing, but very slowly. If deemed necessary, these variations can be tracked using an online monitoring and parameter adaptation algorithm.

V. Simulations and Experiments

As mentioned in Remark 2, the assumptions on which the stability proof is based represent a somewhat idealized scenario. Particularly, the method for reference computation in the previous section has somewhat different dynamic properties than the ideal (13) and (14). Verification is therefore important; this has been made through experiments using a scaled-down three-phase MMC prototype, see Fig. 2, and also through simulations using an averaged model with data identical to the prototype.

Several experimental results vindicating the stability properties were presented already in [28], for the same prototype MMC, i.e., including a measurement lag. These experiments included operating-point changes. In this section, focus is therefore on the differences to the system in [28], namely:

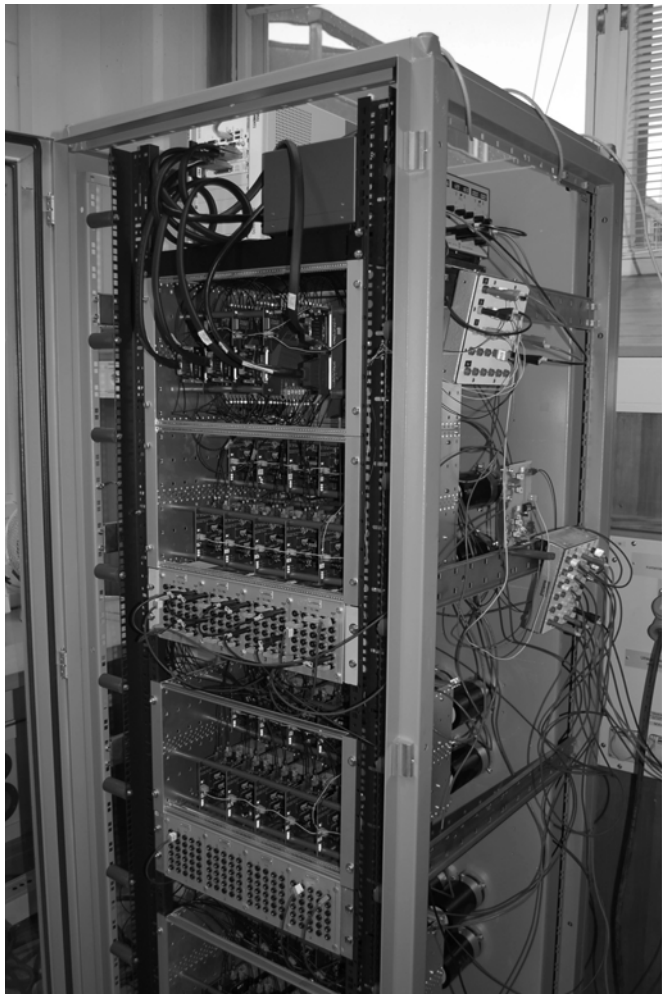

Fig. 2. Photograph of the laboratory setup.

TABLE I
Ratings of the Experimental MMC

DC-bus voltage	$v_d = 500$ V
Peak output voltage	$\hat{v}_s = 225$ V
Peak output current	$\hat{i}_s = 10$ A
Fundamental frequency	$f_1 = 50$ Hz
Switching frequency per submodule	$f_{\rm sw} = 500$ Hz
Number of submodules per arm	$N = 5$
Mean submodule-capacitor voltage	$v_{cu,l0}^i = 100$ V
Submodule capacitance	$C = 0.73$ mF
Arm inductance	$L = 4.7$ mH
Parasitic arm resistance	$R = 0.3\ \Omega$
"Active resistance"	$R_a = 13\ \Omega$

1) the addition of closed-loop circulating-current control;
2) the usage of a different reference-computation method.

Waveforms for phase leg a only will be shown; as the system is balanced, the waveforms for the other two phase legs are identical, but the ac quantities are obviously time shifted corresponding to -120° and -240°, respectively, of the fundamental period. The ratings of the prototype are given in Table I. The measurement time delay is approximately 300 μs, implying

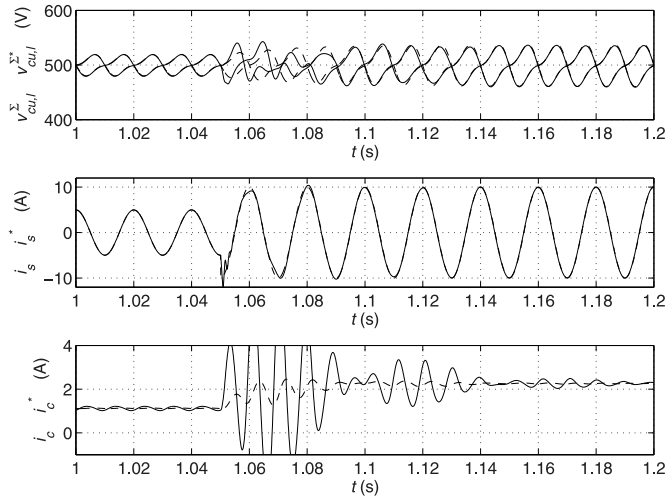

Fig. 3. Simulated step in the output-current reference for $R_a = 0$. Dashed curves are references.

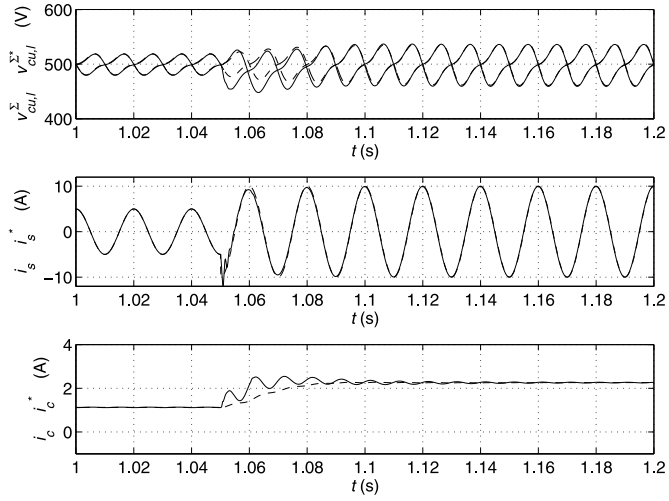

Fig. 4. Simulated step in the output-current reference for $R_a = 13\,\Omega$. Dashed curves are references.

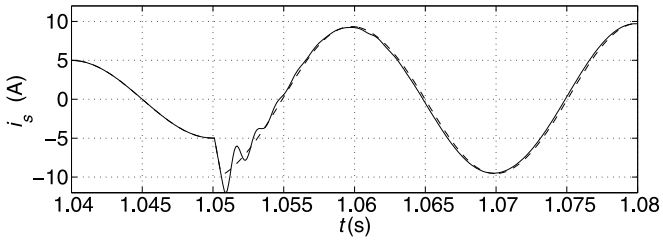

Fig. 5. Simulated step in the output-current reference for $R_a = 13\,\Omega$: (solid) with and (dashed) without a measurement lag.

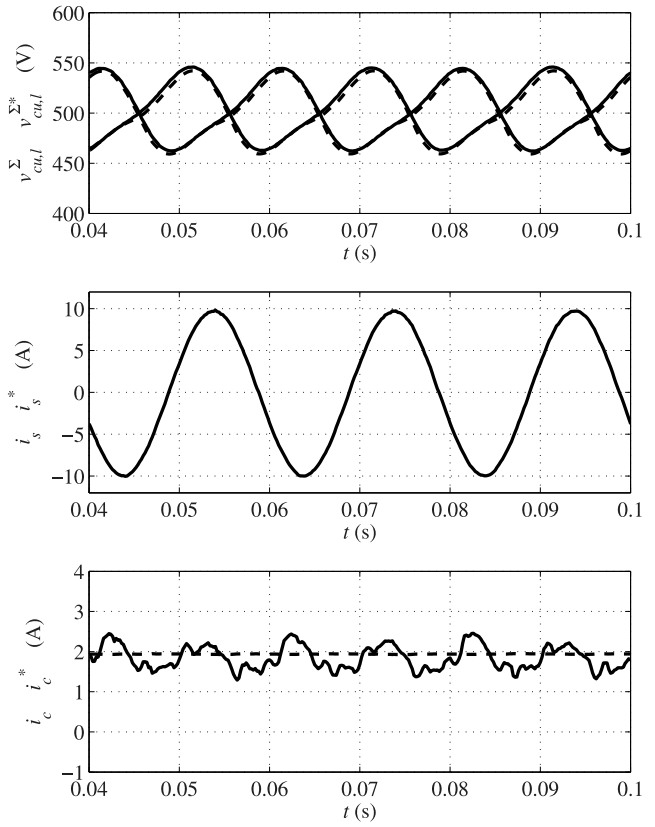

Fig. 6. Experimental results with $R_a = 0$, showing periodic perturbations in the circulating current. Dashed curves are references.

that it can be represented by a lag filter with bandwidth $\alpha_m = 3$ krad/s.

The simulation model and the prototype differ in that the former has a stiff grid voltage—in agreement with the theory—whereas the latter feeds a resistive–inductive load. The inherent damping of experimental system is therefore much higher than that of the simulated system. For the output-current controller, $\alpha_c = 6$ krad/s is used, i.e., twice the lag bandwidth, and for the bandpass filters, $\alpha_f = 50$ rad/s is selected.

First, it is verified that the absence of an "active resistance" leads to poor damping. To avoid that the damping of the prototype's passive load might give too optimistic a result, this verification is made by simulation. Initially, the output-current-reference peak value $\hat{i}_s^\star$ is set to 5 A. After a steady state has been reached, $\hat{i}_s^\star$ is, at $t = 1.05$ s, stepped up to the nominal 10 A. As seen by comparing Figs. 3 and 4, there are significantly larger transient oscillations in the circulating current for $R_a = 0$ than for $R_a = 13\,\Omega$. In addition, there is a noticeable steady-state ripple in the former case. This indicates that the proposed method for computing the sum-capacitor-voltage references, using bandpass filters, is perhaps not perfect, but that its performance can be enhanced by the usage of closed-loop circulating-current control.

Next, a comparison to a converter with a negligible measurement lag is made, which obviously must be made through simulation. In Fig. 5 it is seen that, with a negligible lag there is no ringing in the output current immediately after the step application. However, the ringing in the solid curve is not significant, which shows that the system is tolerant to a measurement lag.

Experimental results will now be presented.

First, an evaluation is made for $R_a = 0$, with results shown in Fig. 6. In agreement with Fig. 3, the circulating current has periodic perturbations, though there are now also higher order harmonics present.

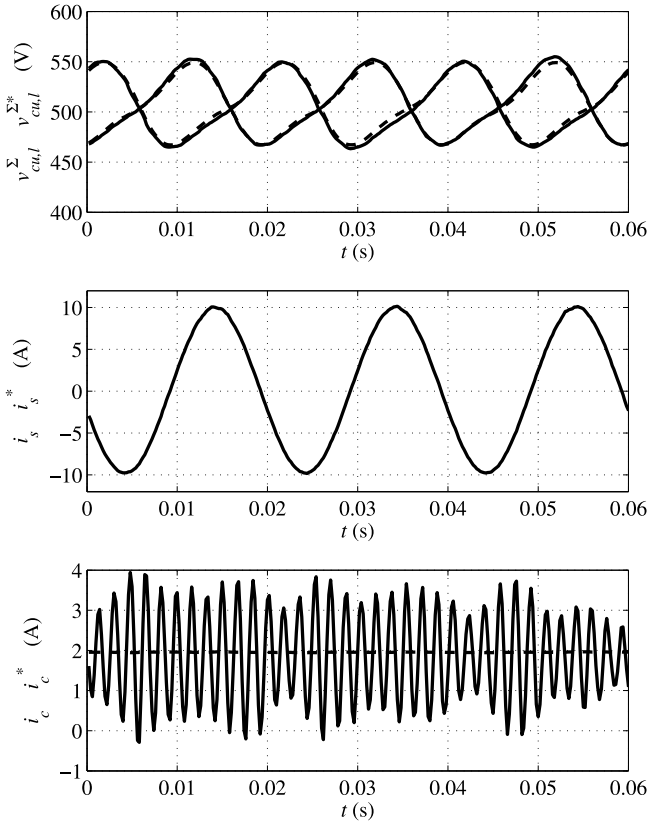

Fig. 7. Experimental results with $R_a = 13\ \Omega$, with arm-energy references computed using closed-form expressions [28], resulting in instability. Dashed curves are references.

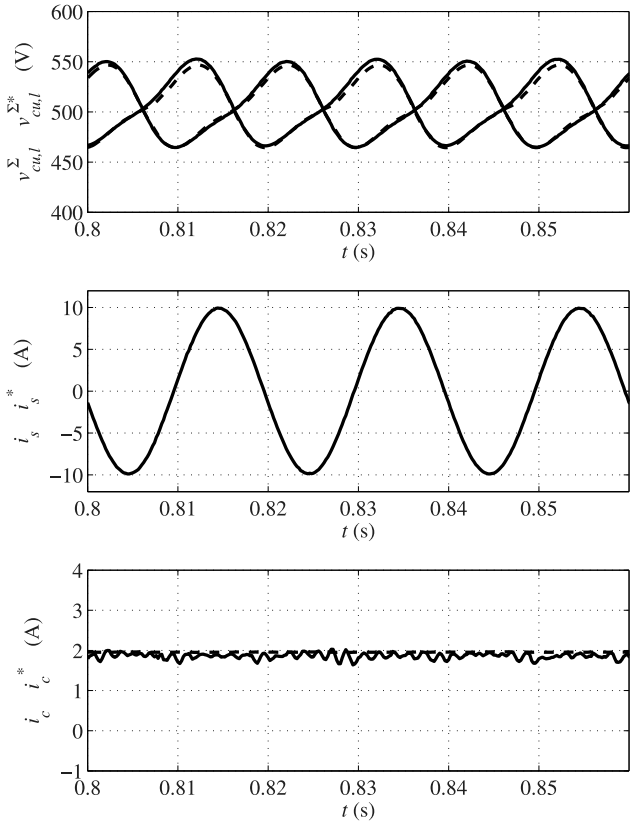

Fig. 8. Experimental results with $R_a = 13\ \Omega$, with the arm-energy references computed using bandpass filtering as shown in Section IV, resulting in asymptotic stability. Dashed curves are references.

Next, circulating-current control with $R_a = 13\ \Omega$ is introduced, but with arm-energy references obtained using the closed-form expressions derived in [28]. Instability results, appearing as an oscillating circulating current, as shown in Fig. 7. The reason for this instability is that the circulating-current feedback in control law (17) is disregarded in the computation of the arm-energy references. The prerequisites of the stability proof are not fulfilled. The instability vanishes if R_a is made smaller; notice that $R_a = 13\ \Omega$ is quite large in relative terms, approximately nine times larger than $X = \omega_1 L = 1.5\ \Omega$ and 43 times larger than $R = 0.3\ \Omega$.

Finally, (50) and (51) are used for computing the arm-energy references (with integration and bandpass filtering implemented using a resonant filter [35]). The resulting output and circulating currents are displayed in Fig. 8. It is seen that, using the method proposed in Section IV, stability is achieved even with the large $R_a = 13\ \Omega$. Furthermore, in agreement with the simulation results, an "active resistance" significantly reduces the periodic perturbations in the circulating current, cf. Fig. 6.

VI. Conclusion

Global asymptotic stability of open-loop voltage control of the MMC, augmented with closed-loop circulating-current control and taking the output-current control loop and a first-order measurement lag into consideration, was proven. Whereas in [28], closed-form expressions were derived for the sum-capacitor-voltage references, in this paper the latter are computed online using bandpass filters and integration. This modification was found crucial to stability for higher values of the circulating-current control gain (the "active resistance"). Although the usage of bandpass filters formally violates the assumptions on which the stability proof is based, this violation was—unlike the usage of closed-form expressions—in simulations and experiments found not to be significant enough to alter the stability properties.

References

[1] J.-S. Lai and F. Z. Peng, "Multilevel converters—A new breed of power converters," *IEEE Trans. Ind. Appl.*, vol. 32, no. 3, pp. 509–517, May 1996.

[2] J. Rodriguez, J.-S. Lai, and F. Z. Peng, "Multilevel inverters: A survey of topologies, controls, and applications," *IEEE Trans. Ind. Electron.*, vol. 49, no. 4, pp. 724–738, Aug. 2002.

[3] A. Lesnicar and R. Marquardt, "An innovative modular multilevel converter topology suitable for a wide power range," presented at the *IEEE Bologna Power Tech*, Bologna, Italy, 2003, vol. 3

[4] A. Lesnicar and R. Marquardt, "A new modular voltage source inverter topology," presented at the *Eur. Conf. Power Electron. Appl.*, Toulouse, France, 2003

[5] M. Glinka and R. Marquardt, "A new single-phase ac/ac-multilevel converter for traction vehicles operating on ac line voltage," presented at the *Power Electron. Appl.*, Toulouse, France, 2003

[6] M. Glinka and R. Marquardt, "A new ac/ac-multilevel converter family applied to a single-phase converter," in *Proc. Power Electron. Drive Syst.*, Singapore, Nov. 2003.

[7] A. Lesnicar, J. Hildinger, and R. Marquardt, "Modulares Stromrichterkonzept für Netzkupplungsanwendungen bei hohen Spannungen,"

(in German) in *Proc. ETG-Fachbericht*, Bad Nauheim, Germany, Apr. 2002, vol. 88, pp. 155-161.
[8] M. Glinka, "Prototype of multiphase modular-multilevel-converter with 2 MW power rating and 17-level-output-voltage," in *Proc. IEEE Power Electron. Spec. Conf.*, vol. 4, Aachen, Germany, Jun. 2004, pp. 2572–2576.
[9] M. Glinka and R. Marquardt, "A new ac/ac multilevel converter family," *IEEE Trans. Ind. Electron.*, vol. 52, no. 3, pp. 662–669, Jun. 2005.
[10] M. Hagiwara and H. Akagi, "Control and experiment of pulsewidth-modulated modular multilevel converters," *IEEE Trans. Power Electron.*, vol. 24, no. 7, pp. 1737–1746, Jul. 2009.
[11] S. Allebrod, R. Hamerski, and R. Marquardt, "New transformerless, scalable modular multilevel converters for HVDC-transmission," in *Proc. IEEE Power Electron. Spec. Conf.*, 2008, pp. 174–179.
[12] D. Peftitsis, G. Tolstoy, A. Antonopoulos, J. Rabkowski, J.-K. Lim, M. Bakowski, L. Ängquist, and H.-P. Nee, "High-power modular multilevel converters with SiC JFETs," *IEEE Trans. Power Electron.*, vol. 27, no. 1, pp. 28–36, Jan. 2012.
[13] M. Saeedifard and R. Iravani, "Dynamic performance of a modular multilevel back-to-back HVDC system," *IEEE Trans. Power Del.*, vol. 25, no. 4, pp. 2903–2912, Oct. 2010.
[14] M. Hiller, D. Krug, R. Sommer, and S. Rohner, "A new highly modular medium voltage converter topology for industrial drive applications," presented at the *Eur. Conf. Power Electron. Appl.*, Barcelona, Spain, 2009
[15] A. Antonopoulos, K. Ilves, L. Ängquist, and H.-P. Nee, "On interaction between internal converter dynamics and current control of high-performance high-power ac motor drives with modular multilevel converters," in *Proc. IEEE Energy Convers. Congr. Expo.*, 2010, pp. 4293–4298.
[16] M. Hagiwara, K. Nishimura, and H. Akagi, "A medium-voltage motor drive with a modular multilevel PWM inverter," *IEEE Trans. Power Electron.*, vol. 25, no. 7, pp. 1786–1799, Jul. 2010.
[17] A. J. Korn, M. Winkelnkemper, and P. Steimer, "Low output frequency operation of the modular multi-level converter," in *Proc. IEEE Energy Convers. Congr. Expo.*, 2010, pp. 3993–3997.
[18] M. Winkelnkemper, A. Korn, and P. Steimer, "A modular direct converter for transformerless rail interties," in *Proc. IEEE Symp. Ind. Electron.*, 2010, pp. 562–567.
[19] L. Ängquist, A. Haider, H.-P. Nee, and H. Jiang, "Open-loop approach to control a modular multilevel frequency converter," presented at the *Eur. Conf. Power Electron. Appl.*, Birmingham, U.K., 2011
[20] S. Rohner, S. Bernet, M. Hiller, and R. Sommer, "Modulation, losses, and semiconductor requirements of modular multilevel converters," *IEEE Trans. Ind. Electron.*, vol. 57, no. 8, pp. 2633–2642, Aug. 2010.
[21] A. Antonopoulos, L. Ängquist, and H.-P. Nee, "On dynamics and voltage control of the modular multilevel converter," presented at the *Eur. Conf. Power Electron. Appl.*, Barcelona, Spain, 2009
[22] M. A. Pérez and J. Rodríguez, "Generalized modeling and simulation of a modular multilevel converter," in *Proc. IEEE Symp. Ind. Electron.*, 2011, pp. 1863–1868.
[23] M. Hagiwara, R. Maeda, and H. Akagi, "Control and analysis of the modular multilevel cascade converter based on double-star chopper-cells (MMCC-DSCC)," *IEEE Trans. Power Electron.*, vol. 26, no. 6, pp. 1649–1658, Jun. 2011.
[24] L. Ängquist, A. Antonopoulos, D. Siemaszko, K. Ilves, M. Vasiladiotis, and H.-P. Nee, "Open-loop control of modular multilevel converters using estimation of stored energy," *IEEE Trans. Ind. Appl.*, vol. 47, no. 6, pp. 2516–2524, Nov./Dec. 2011.
[25] Q. Tu, Z. Xu, and L. Xu, "Reduced switching-frequency modulation and circulating current suppression for modular multilevel converters," *IEEE Trans. Power Del.*, vol. 26, no. 3, pp. 2009–2017, Jul. 2011.
[26] M. A. Pérez, J. Rodríguez, E. J. Fuentes, and F. Kammerer, "Predictive control of ac-ac modular multilevel converters," *IEEE Trans. Ind. Electron.*, vol. 59, no. 7, pp. 2832–2839, Jul. 2012.
[27] L. Harnefors, A. Antonopoulos, S. Norrga, L. Ängquist, and H.-P. Nee, "Dynamic analysis of modular multilevel converters," *IEEE Trans. Ind. Electron.*, vol. 60, no. 7, pp. 2526–2537, Jul. 2013.
[28] A. Antonopoulos, L. Ängquist, L. Harnefors, K. Ilves, and H.-P. Nee, "Global asymptotic stability of modular multilevel converters," *IEEE Trans. Ind. Electron.*, vol. 61, no. 2, pp. 603–612, Feb. 2014.
[29] L. Harnefors, A. Antonopoulos, and H.-P. Nee, "Global asymptotic stability of modular multilevel converters with measurement lag and circulating-current control," in *Proc. Eur. Conf. Power Electron. Appl.*, Lille, France, 2013, pp. 1–10.
[30] L. Harnefors and H.-P. Nee, "Model-based current control of ac machines using the internal model control method," *IEEE Trans. Ind. Appl.*, vol. 34, no. 1, pp. 133–141, Jan./Feb. 1998.
[31] L. Harnefors, L. Zhang, and M. Bongiorno, "Frequency-domain passivity-based current controller design," *IET Power Electron.*, vol. 1, no. 4, pp. 455–465, Dec. 2008.
[32] R. Teodorescu, F. Blaabjerg, M. Liserre, and P. C. Loh, "Proportional-resonant controllers and filters for grid-connected voltage-source converters," *IEE Proc.—Electr. Power Appl.*, vol. 153, no. 5, pp. 750–762, Sep. 2006.
[33] H. K. Khalil, *Nonlinear Systems*, 3rd ed. Upper Saddle River, NJ, USA: Pearson Education, 2003.
[34] N. Mohan, T. Undeland, and W. P. Robbins, *Power Electronics: Converters, Applications, and Design*, 3rd ed. New York, NY, USA: Wiley, 2002.
[35] L. Harnefors, "Implementation of resonant controllers and filters in fixed-point arithmetic," *IEEE Trans. Ind. Electron.*, vol. 56, no. 4, pp. 1273–1281, Apr. 2009.

Lennart Harnefors (S'93–M'97–SM'07) was born in 1968 in Eskilstuna, Sweden. He received the M.Sc., Licentiate, and Ph.D. degrees in electrical engineering from the Royal Institute of Technology (KTH), Stockholm, Sweden, and the Docent degree in industrial automation from Lund University, Lund, Sweden, in 1993, 1995, 1997, and 2000, respectively.

From 1994 to 2005, he was with Mälardalen University, Västerås, Sweden, where he held the positions of Research Assistant, Senior Lecturer, and, from 2001, Professor. He served as Head of the Systems, Control, and Power Engineering Laboratory from 1998 to 2004. Between 2001 and 2005, he was, in addition, a part-time Visiting Professor of electrical drives with Chalmers University of Technology, Göteborg, Sweden. Since 2005, he has been with ABB, where he served in various capacities at the Grid Systems/HVDC business unit 2005–2012. Currently, he is a Senior Principal Scientist at Corporate Research, Västerås, Sweden. He is working part time with KTH as an Adjunct Professor of power electronics. His research interests include analysis and control of power electronic systems, particularly grid-connected converters and ac drives.

Prof. Harnefors received the 2000 ABB Gunnar Engström Energy Award and the 2002 IEEE TRANSACTIONS ON INDUSTRIAL ELECTRONICS Best Paper Award. He is an Associate Editor of the IEEE TRANSACTIONS ON INDUSTRIAL ELECTRONICS, a Member of the Editorial Board of *IET Electric Power Applications*, and a Member of the Executive Council and the International Scientific Committee of the European Power Electronics and Drives Association. He is the author of more than 100 papers and holds five granted patents with several more pending.

Antonios Antonopoulos (S'06) was born in Athens, Greece, in 1984. He received the Diploma of electrical and computer engineering from the National Technical University of Athens, Athens, Greece, in 2007, and his Licentiate degree in electrical engineering from the Royal Institute of Technology (KTH), Stockholm, Sweden in 2011. Since 2008, he is working toward the Ph.D. degree with the Electrical Energy Conversion Laboratory, KTH.

His major research interests include high-power-electronic converters for large- and medium-scale motor drives and grid applications.

Kalle Ilves (S'10) received the M.Sc. and Licentiate degrees in electrical engineering from the Royal Institute of Technology (KTH), Stockholm, Sweden, in 2009 and 2012, respectively. Since 2010, he is working toward the Ph.D. degree at the Electrical Energy Conversion Laboratory at KTH.

His major research interests include high-power converters for grid applications.

Mr. Ilves received a Best Paper Award at the IEEE 7th International Power Electronics and Motion Control Conference ECCE Asia, Harbin, China.

Hans-Peter Nee (S'91–M'96–SM'04) was born in Västerås, Sweden, in 1963. He received the M.Sc., Licentiate, and Ph.D. degrees in electrical engineering from the Royal Institute of Technology (KTH), Stockholm, Sweden, in 1987, 1992, and 1996, respectively.

In 1999, he was appointed Professor of power electronics at KTH, where he currently serves as the Head of the Electrical Energy Conversion Laboratory. His current research interests include power electronic converters, semiconductor components, and control aspects of utility applications, such as flexible ac transmission systems, high-voltage dc transmission, and variable-speed drives.

Prof. Nee received the Energy Prize by the Swedish State Power Board in 1991, the ICEM'94 (Paris) Verbal Prize in 1994, the Torsten Lindström Electric Power Scholarship in 1996, and the Elforsk Scholarship in 1997. He is a Member of the European Power Electronics and Drives Association, involved with the Executive Council and the International Scientific Committee. He is also an Associate Editor of the IEEE TRANSACTIONS ON POWER ELECTRONICS and was on the Board of the IEEE Sweden Section for several years, serving as its Chairman during 2002–2003.